Studies on background PFC and current distribution using individual anode signals in aluminium reduction cells

Ali Jassim[1], Sergey Akmetov[2], Barry Welch[3], Maria Skyllas-Kazacos[4], Jie Bao[5] and Yuchen Yao[6]
1. General Superintendent – Process Control
2. Vice President, Reduction
Emirates Global Aluminium, Jebel Ali Operations, P.O. Box 3627, Dubai, U.A.E.
3. Emeritus Professor
4. Emeritus Professor
5. Professor
6. Ph.D. Student
The University of New South Wales, Sydney, Australia, 2052
Corresponding author: abanjab@ega.ae

Abstract

The growing world demand on aluminium has encouraged modern smelters to increase their production output through increasing operating amperage together with proportional increase in anode size to maintain acceptable anode current density. Though, the increase in anode size was outweighed with a reduction in molten electrolyte volume which added a stress on process of alumina mixing and dissolution in bath. Under such condition, convectional cell control signal which is cell volt cannot detect variation in cell spatial and temporal condition which causes non-uniform current density whilst at high anode potential; the anode reaction product could change to include the co-evolution of PFC species. In this paper, individual anode current signals were used to study the impact of anode stall location on its current pick up curve whilst a complimentary time and frequency domain analysis is conducted. A detailed analysis for the impact of changes in cell spatial condition which result in the increase co-evolution of carbon monoxide (CO) and fluorocarbon species namely tetrafluoride CF_4 emissions is studied.

1. Introduction

The continuous increase in modern Hall-Héroult electrolysis cell amperage rating has been combined with a reduction in cell inter-electrode distance aiming for lower energy consumption whilst operating with an increase anode size to maintain acceptable current density. Accordingly, a reduction in total available molten electrolyte volume in the cell has occurred where at higher rates of daily alumina dumps, the process of steady alumina dissolution process has become a challenge. Under conditions of low energy input, there is an increased tendency to form local spatial abnormalities that lead to the co-evolution of fluorocarbon species where anodes are partially passivated but cannot be monitored by convectional cell control algorithms which rely on the measured cell voltage signal. Previous studies [1] have shown that the rate of current pick-up for newly set anodes decreases as anode size increase resulting in a prolonging of the period of operating under non-uniform current distribution and high magnetohydrodynamic (MHD) instability. Management in modern smelters aims to maintain the same number of feeders while increasing cell amperage and dimension to maintain lower costs. This however adds an extra challenge for the homogeneous alumina dispersion and mixing in the electrolyte. The work in this paper is divided into two parts, the first of which describes a detailed study to understand the impact of anode stall location on characterising the current pick-up curves for newly set anodes where the different chemical kinetics, local MHD and heat transfer process between molten electrolyte and anode interface play a dominant role in controlling anode current evolution. The second part of the work studies changes in individual anode current signals while introducing a spatial variation in cell condition such as blocking a feeder or creating an imbalance in anode current distribution which results in the co-evolution of fluorocarbon

species. Sequentially, the work illustrates the broad potential of using individual anode currents as an aid for early fault diagnostics for operating cells.

2. Part 1: Anode setting analysis

The aluminium electrowinning process given in reaction (1) is responsible for 75 % of carbon consumption in the Hall-Heroult process [2]:

$$2Al_2O_{3\,(diss)} + 3C = 4Al_{(l)} + 3CO_{2(g)} \quad (1)$$

Discharged oxygen atoms from the active surface of alumina react with the anode carbon electrode producing carbon dioxide at the anode and liquid aluminium at the cathode.

Mechanisms that account for the remaining 25 % of carbon consumption are associated with the air burn reaction, the boudouard reaction and carbon dusting where selective wearing of anode components occurs resulting in detachment of unreacted particles from the anode surface. Accordingly, the combined effect of various anode consumption mechanisms result in reducing anode height to a minimum operating level typically after 25 - 30 days of setting after which the carbon anodes are replaced to avoid contamination of produced liquid aluminium by impurities from the anode yoke. A new anode is replaced every 1 - 3 days causing MHD instability and losses in process efficiency [3] as a result of subsequent disturbance in cell thermal and electric balance, with the new anode requiring 6-8 days to achieve steady anode current draw and hence current distribution [4]. Modern cells are designed to operate with a balanced anode current distribution while under low energy operating conditions, current pick-up curves become more individualistic based on anode stall location.

2.1. Methodology of analysing anode current evolution based on anode stall location

Massive disturbances in anode cell thermal balance occur due to local energy deficits during anode setting, resulting in formation of a frozen bath layer which hinders current flow and alumina dispersion in the vicinity of the replaced anodes. While temperature distribution simulations reported by Cheung et al showed a higher operating temperature toward the central anodes [5], characteristic changes in the rate of current pick-up based on anode stall location was rarely covered in literature.

In the present study, more than 207 anode current curves were analysed and central anodes showed a faster average rate of current pick-up compared to corner anodes as shown in Figure 1.

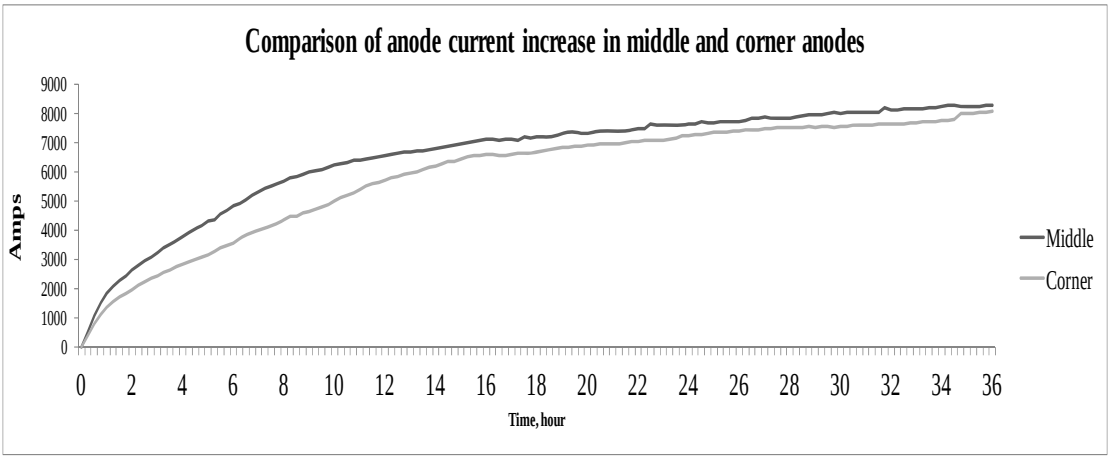

Figure 1. Actual average anode current profile for corner and central anodes.

This can be explained by the fact that central anodes operate at higher bath superheat due to better convectional heat transfer from the electrolyte and radiated energy from neighbouring hot anodes coupled with lower inter-electrode distance due to marginally higher metal pad which offers lower ohmic path resistance for current.

Besides, the location of central anodes closer to point feeders ensures adequate alumina supply that is received from either one or two feeders, as shown in Figure 2, which assist in lowering anode potential [6, 7].

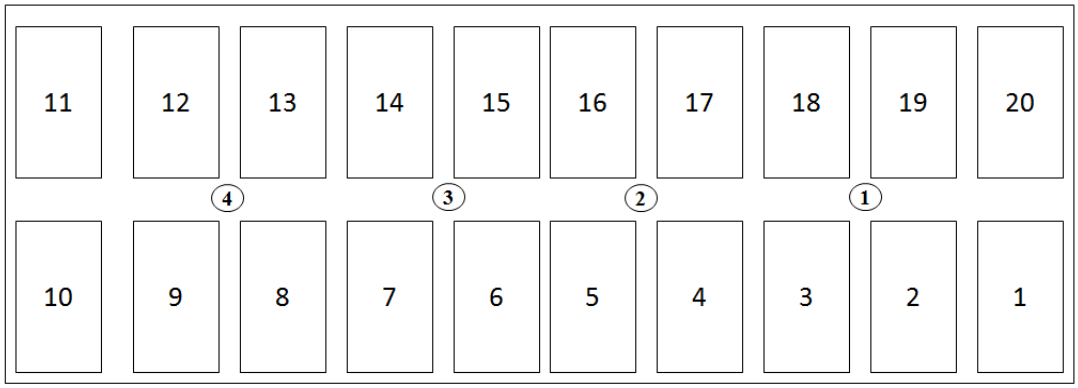

Figure 2. Layout of anode and feeders in tested industrial cell.

The different rates of current increase of central and corner anodes are compared in Figure 3 which shows that the central anode current rate significantly exceeds corner anode current rate in the initial 14 hours of operation that is mainly controlled by the freeze dissolution process [8].

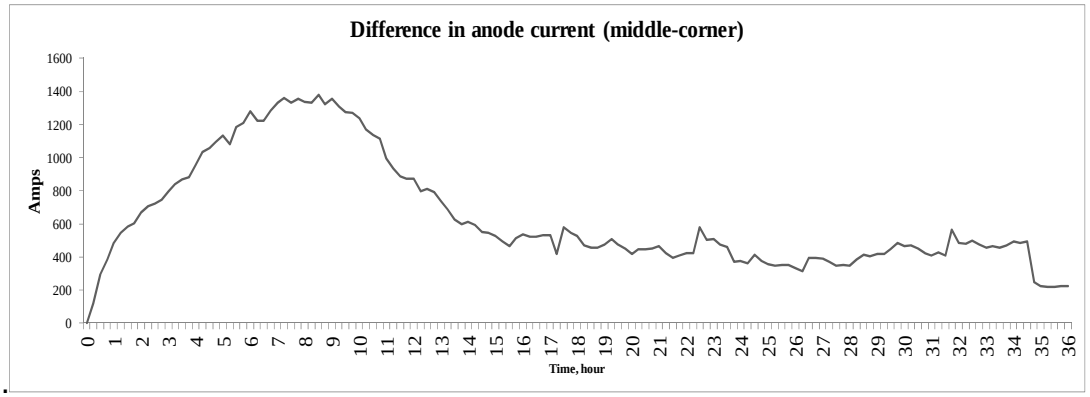

Figure 3. Difference in anode current between middle and corner anodes.

As shown in Figure 4, the MHD model for the cell during replacement of the centre and corner anodes has shown that the central anodes operate under lower ACD during replacement which allows for higher current flow.

Thermodynamically, changes in individual anodes ACD apply a different entropic cooling effect during anode replacement. Anodes experience a negative entropic cooling energy corresponding to - 0.705 V while evolving CO_2 and - 1.249 V while evolving CO at 960 °C which introduces local energy deficit [10]. During anode setting, a total heat deficit of 6700 W/m² occurs at the anode surface due to the combined effect of entropic cooling, anodic overvoltage and upward heat flux from the anode block, with the required energy extracted from bath [11]. Corner anodes undergo a higher heat loss due to lower heating entropic energy as a result of a slower increase in current density. Furthermore, the higher heat loss

due to radiated heat from the side wall to the environment increases the local heat deficit while replacing corner anodes. In contrast, the improved superheat in the vicinity of central anodes [5] reduces the impact of the energy shortfall during anode setting, resulting in a faster current rise.

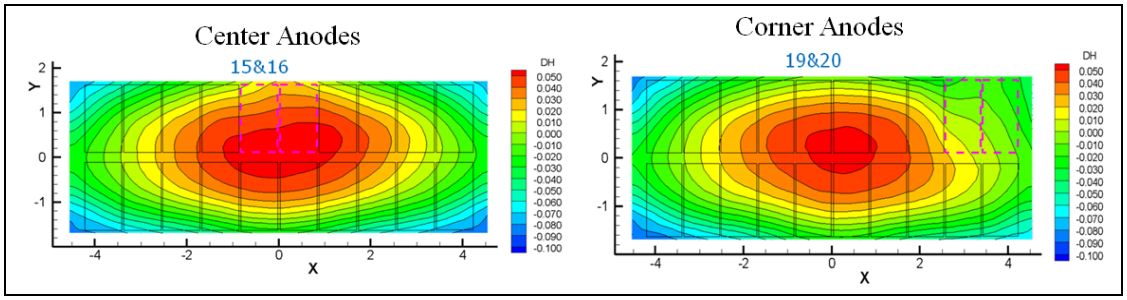

Figure 4. MHD model of changes in metal prolife contour following replacement corner and central pair of anodes [9].

2.2. Changes in bubble dynamics while setting corner and central anodes

Changes in local cell conditions such as superheat and anode-cathode distance affect the current density of a newly set anode and its bubble release frequency [12]. The thickness of the anode bubble layer under each anode is proportionally characterized by operating current density. Other factors such as electrolyte velocity, anode bottom material microstructure and shape play an important role in the bubble release profile and dynamics [13]. In this work, changes in slotted anode bubble dynamics during setting of corner and centre anode was studied after 1, 8 and 12 hours of anode replacement.

2.3. Bubble frequency spectrum analysis

Fast Fourier Transform (FFT) analysis of bubble dynamics for corner and central anode was conducted at different time intervals after anode setting while the individual anode current data were sampled at a high frequency of 200 Hz. Analysis showed different bubble power spectra at the different studied intervals. In the first one hour while both anodes operate at low current density, a low frequency bubble peak is observed in the corner anode, as demonstrated in Figure 5, and is attributed to the low local superheat condition which induces local MHD instability. In contrast, the middle anode did not show the characteristic peak in bubble dynamic probably due to relative better superheat and thus improved MHD stability.

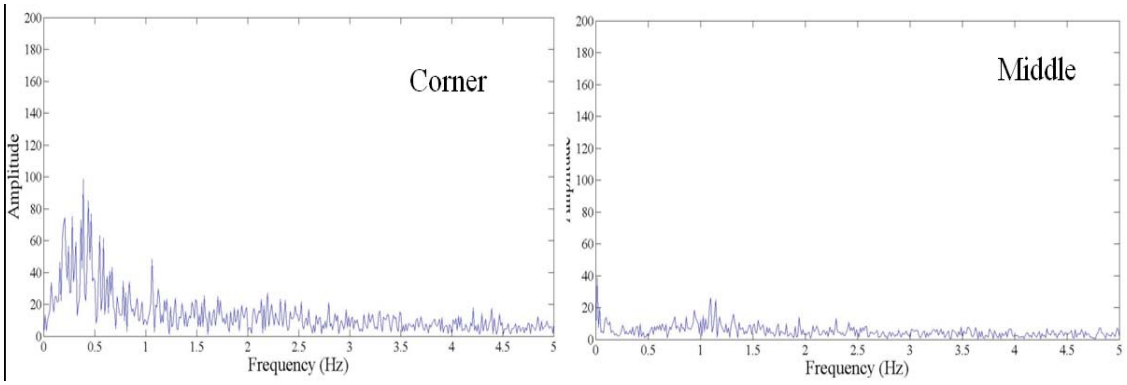

Figure 5. Frequency response of new corner and centre anodes after 1 hour of setting.

Increased current draw in both anodes after 8 hours is a result of accelerated freeze dissolution process and improved local superheat. However, the corner anode still shows a bubble peak in rang of 0.5 - 1.5 Hz as shown in Figure 6 which is attributed due to coverage of corner anode slots by quenched freeze layer that increases coalesced bubble residence time

while detaching to electrolyte. In the same time frame, centre anodes show a low intensity bubble peak in the 0.5 - 1.5 Hz range where the slots allow for faster bubble release.

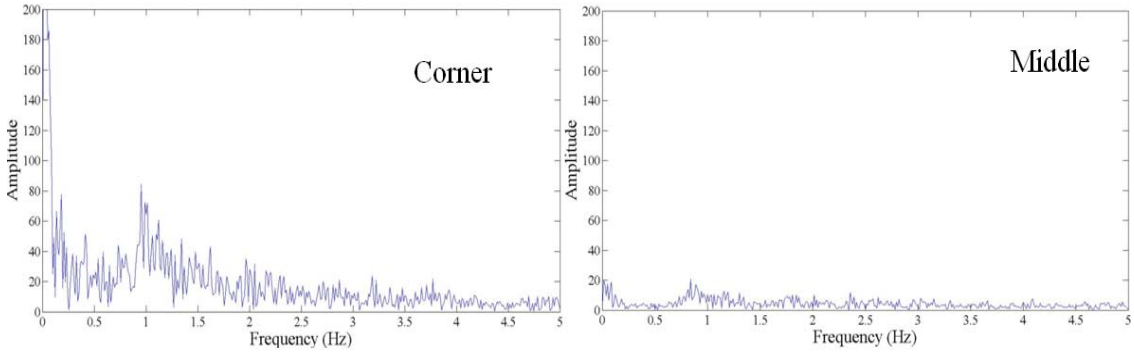

Figure 6. Frequency response of new corner and centre anodes after 8 hour of setting.

The virtually complete freeze melting process in both directions, anode bottom and side after 12 hours of setting, allows for higher current pick-up rate. In conjunction, the efficiency of slots in both anodes is projected to improve whilst the generated bubbles easily detach to the electrolyte, as is reflected by the low bubble spectrum in Figure 7. Nevertheless, a low intensity bubble peak at 0.5 - 1.5 Hz appeared in the corner anode which may indicate the existence of some freeze component due to local entropic cooling which hinders bubble release from the slots.

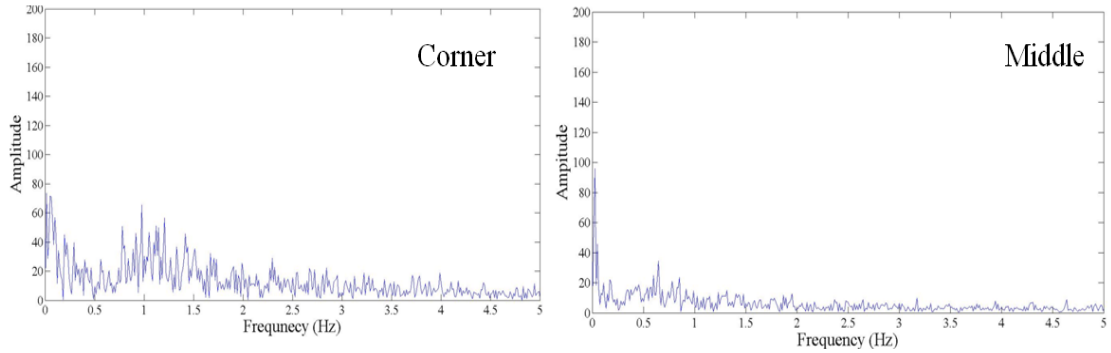

Figure 7. Frequency response of new corner and centre anodes after 12 hour of setting.

Anode bubble dynamics for the corner and middle anodes after 20 hours of setting when the corner anode carries 60 % and the centre anode 71 % of their target load, showed a comparable low bubble spectrum as the generated gas bubbles steadily escapes from the vertical inclined slots to the electrolyte [14] as illustrated in Figure 8.

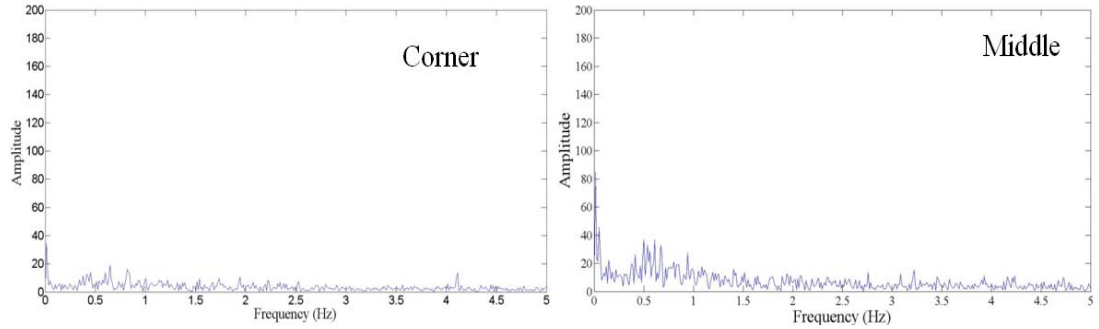

Figure 8. Frequency response of new corner and centre anodes after 20 hour of setting.

The continuous electrochemical consumption of the anode reduces its height and results in disappearance of the slots after 13 - 14 days. The resulting flat anode surface will show increasing bubble resistance and bubble residence time as the bubbles travel horizontally

across the anode bottom plane prior of escaping at the side of the anode to the electrolyte. Accordingly, both corner and centre anodes have shown the appearance of the 0.5 - 1.5 Hz bubble dynamic peak following slot disappearance as shown in Figure 9 when the age of both analysed anodes was 19 days.

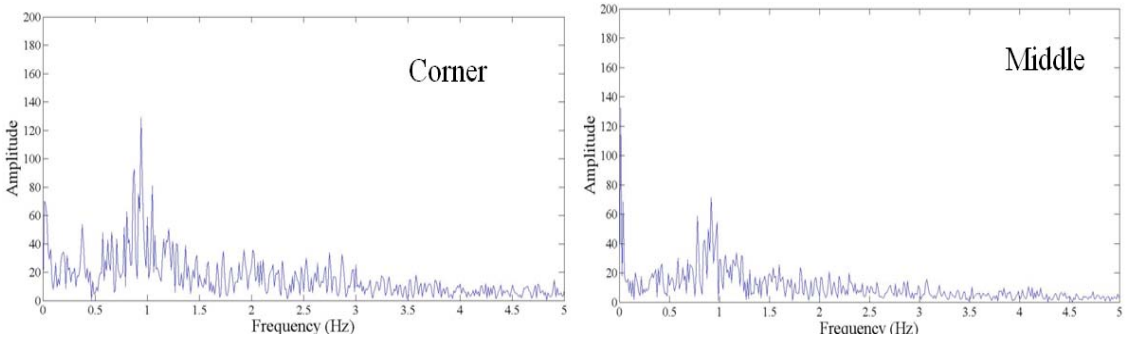

Figure 9. Frequency response of corner and centre anodes after slot disappearance.

3. Part 2: Impact of spatial variation on the co-evolution of fluorocarbon species

3.1. Experiment set up

Experimental investigation was performed on a modern point feed and magnetically compensated cell fitted with individual anode current monitoring system. The cell was installed with Gasmet DX4000 FTIR analyser positioned in the duct of the exhaust gases. To standardise cell operating conditions in all experiments, a set of initial cell parameters was defined prior to starting any experiments where PFC emission were ensured to be at normal level of zero emission. Anode current distributions were ensured to be at balance level with ± 10% variation. Cell average alumina concentration was ensured to be a normal operating level as electrolyte was manually sampled every five minutes. Cell superheat and electrolyte composition was checked to be at normal level between as excess AlF_3 10.5-11.5 % and bath temperature in the range of 958 - 965 °C.

3.2. Studies the impact of alumina concentration gradient on forming non-anode effect PFC emission

The challenge of operating modern cells at low energy input and electrolyte volume [15] is studied in this work by using individual anode current signals. Several publications [16, 17, 18] have shown the impact of increasing alumina concentration gradient while operating at a lower electrolyte volume. Sequentially, an increase in anode potential beyond the enabling limits of the co-evolution of fluorocarbon species permits the formation of bubble resistive film under the anode and reduces anode wettability [18]. In this work, the impact of spatial variations in alumina concentration in the electrolyte across the cell was studied by blocking a corner and middle feeder. The effect of the resultant non-uniform current density distribution on the initiation of PFC emissions was thus analysed for corner and central anodes.

Individual anode electrodes are designed to operate under similar conditions of electrolyte composition and electrode potential. However, because of non-uniform alumina dispersion in the electrolyte, the behaviour of individual anodes will be distinctive with a risk of individual electrode potentials shifting to levels corresponding to the discharge of fluoride ions, with resultant PFC formation.

In the first part of the investigation, feeder 1 of the cell which is shown in Figure 10 was blocked for a period of 20 hours from 12:40 pm to 08:15 am the next day. During this time, the total amount of alumina supply to the cell remained the same while the feeding rate proportionally increased in the other three feeders. An increase in the co-evolution of fluorocarbon species was triggered shortly after 20 minutes of blocking feeder 1 and this was

associated with current redistribution predominately in the anodes around feeder 1. To facilitate the analysis, the cell was divided into four zones based on the feeder's location as illustrated by the different colour scheme in Figure 10.

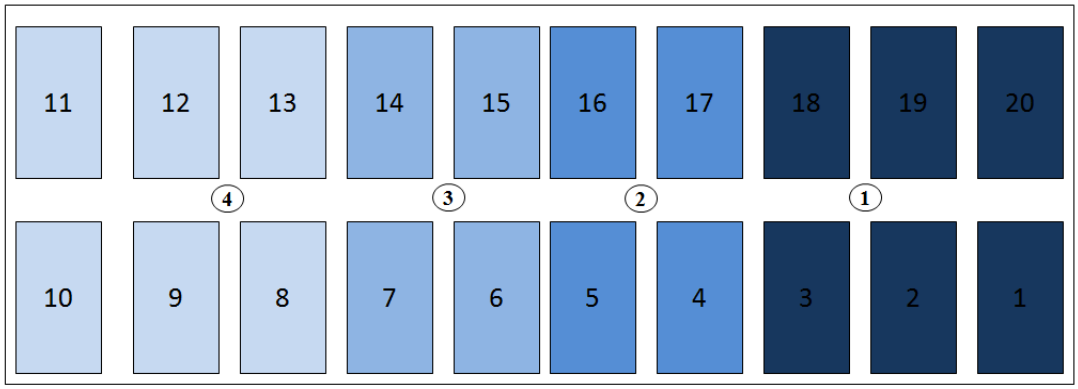

Figure 10. Divided zones in cell based on feeders location while blocking feeder 1 experiment.

The steady depletion of alumina in the vicinity of the anodes near feeder 1 (anodes 1, 2, 3 & 20) has resulted in a lowering of current at these anodes as shown in Figure 11.

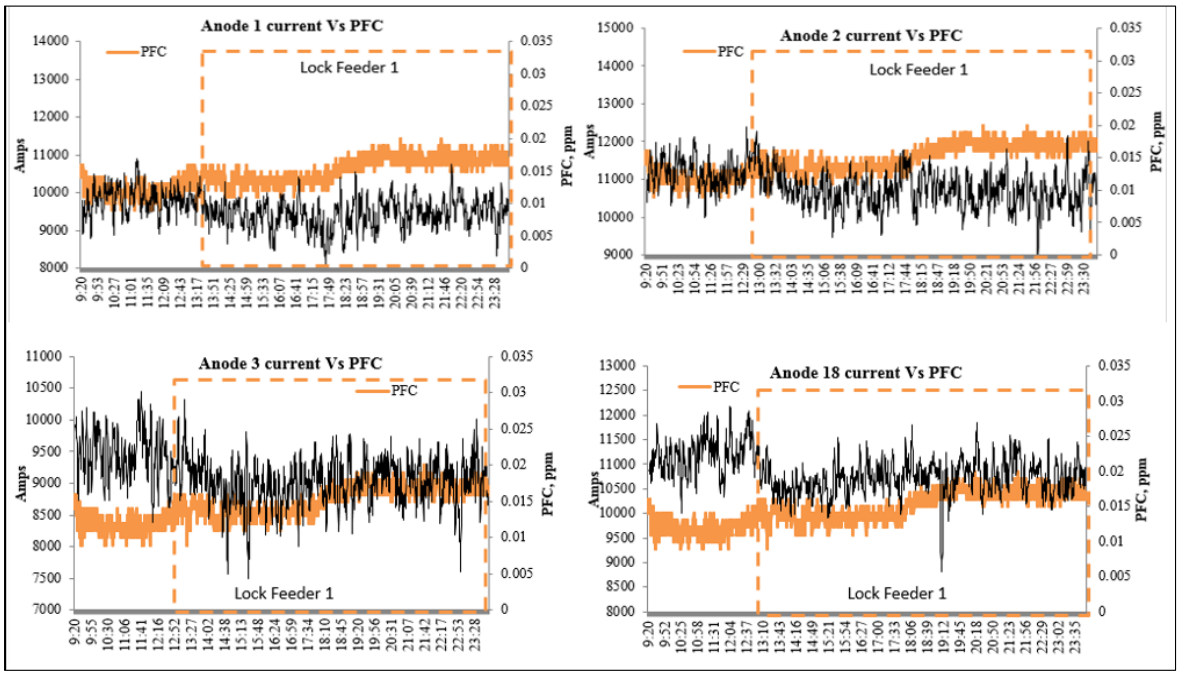

Figure 11. Reduction in anode current for anodes adjacent to feeder 1.

On the other hand, due to constant cell current condition and better alumina concentration in other zones of the cell [19], an increase in current for anodes adjacent to feeder 4 occurred as shown in Figure 12.

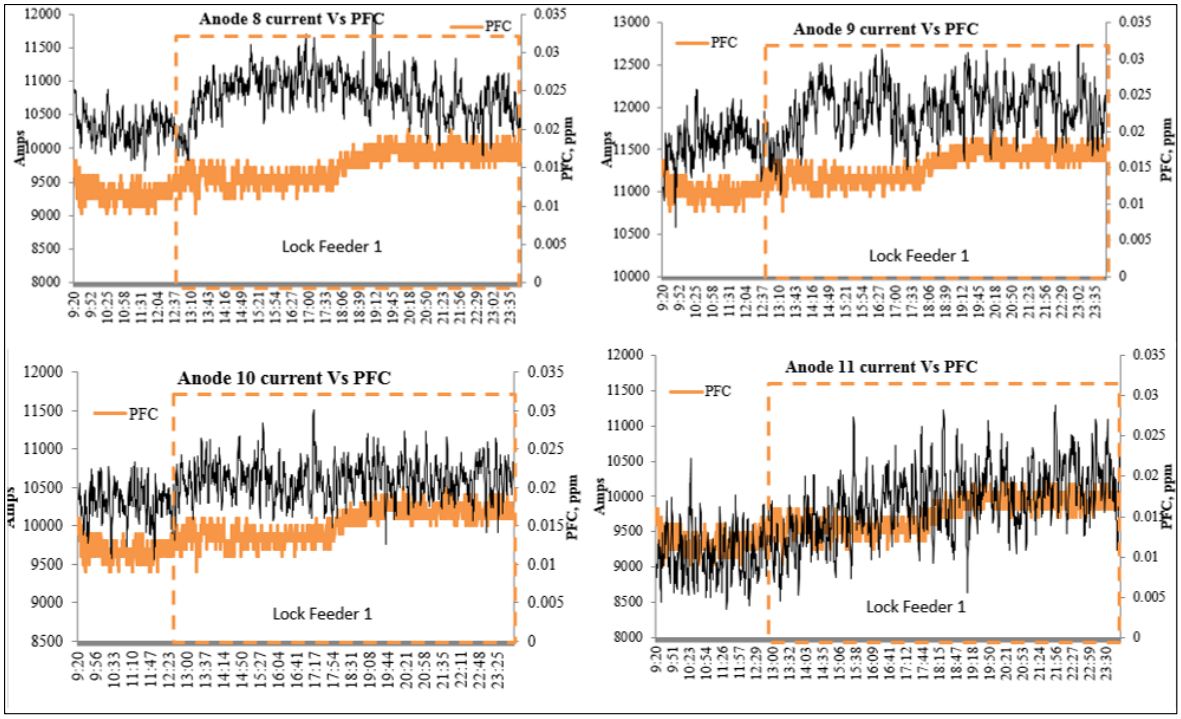

Figure 12. Increase in anode current for anodes adjacent to feeder 4 while blocking feeder 1 experiment.

Alumina concentration analysis while blocking feeder 1 in Figure 13 showed a reduction in alumina content in electrolyte from 3.5 % to 2.5 % which was aligned with the increase in cell PFC emission.

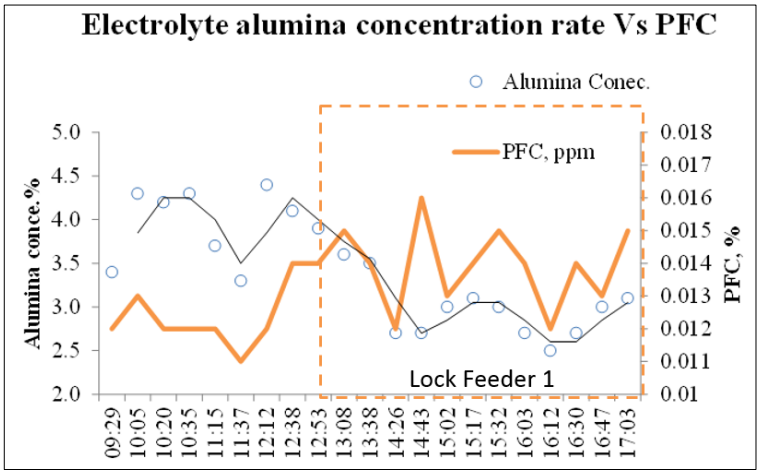

Figure 13. Change in electrolyte alumina concentration and PFC while blocking feeder one experiment.

In the second part of the investigation, feeder 3 was blocked through the cell control unit for 18 hours from 14:10 to 06:00 the next day whilst the total amount of alumina supply to the cell remained the same. Reduction in alumina concentration under anodes adjacent to feeder 3 lowers their wettability and reduces effective surface area that induced a subsequent increase in anode current density where ultimately a fluorinated carbon layer would form under the anodes [20], This results in a partial reduction in anode current as observed for anodes 6 and 7 in Figure 14. The depletion of oxide ions under the anodes causes fluoride containing species in the electrolyte to discharge at the anode and form PFC gases as CF_4 [21].

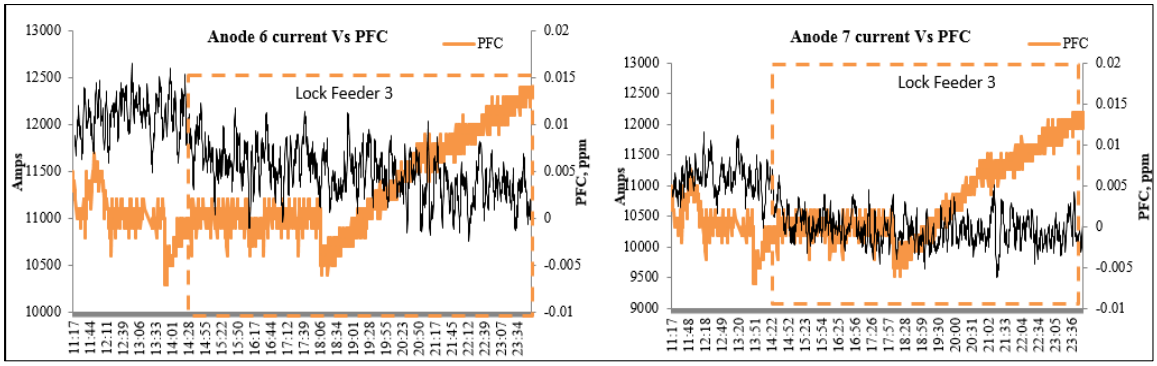

Figure 14. Reduction in anode current of anodes adjacent to feeder 3 while blocking feeder 3 experiment.

The increase in PFC emission during blockage of feeder 3 was relatively slower when compared with blocking feeder 1. Thus, the PFC emission was triggered after 4 hours of blocking feeder 3 whereas it was detected after 20 minutes of blocking feeder 1. Variances in initial condition of alumina concentration in molten electrolyte and positioning feeder 3 in the middle of the cell where adjacent anodes would still receive alumina from other nearby secondary feeders slows alumina depletion rate, whereas at corner anodes, alumina supply is limited from a single corner feeder [22].

3.3. Study of the impact of non-uniform current density on the co-evolution of fluorocarbon species

In the next part of the investigation, the impact of an uneven current distribution on the co-evolution of fluorocarbon species was studied through two independent tests in which pairs of corner and middle anodes were raised respectively. In the first experiment, the uniformity of current distribution was disturbed through raising duct anodes 11 and 12 by 2.5 cm. An abrupt increase in PFC was observed shorty after raising both anodes as their current lowered by 43-48% while current was diverted to other anodes causing an increase in their anode current density. The variation in anode current load and hence higher alumina depletion rate under certain anodes will result in a condition whereby the rate of depletion of oxide ions exceeds the rate of alumina supply. As the anode becomes polarised the voltage reaches the decomposition potential for fluoride ions. Consequently, the carbon anode will react with fluoride species in the electrolyte to form an insulating C-F gas film under anodes at higher anode potential, thereby severely increasing anode resistance [23]. Anodes adjacent to raised anodes 11 and 12 experienced an initial increase in current but once PFC emission was initiated in the cell, their current starts to show partial reduction, as observed for anodes 9, 10, 13 and 14 in Figure 15.

Changes in individual anode currents in the period of two hours before and after commencing the experiment are presented in Figure 16. The analysis shows the biggest increase in current occurred in anodes 3, 4 and 5 around feeders 1 and 2.

The general explanation for changes in anode current while positioning anodes 11 and 12 at a higher reference would be supported by a similar situation while setting them since new anodes are set at equivalent higher levels than the reference position to allow adequate heating period. The MHD model corresponding to anode 11 and 12 replacement was analysed in Figure 17 which shows that anodes 3, 4 and 5 are located under a high metal velocity and lower ACD region which would allow higher heat transfer from the metal [24] and provide a better bath mixing condition [25] which in turn allows for higher current share.

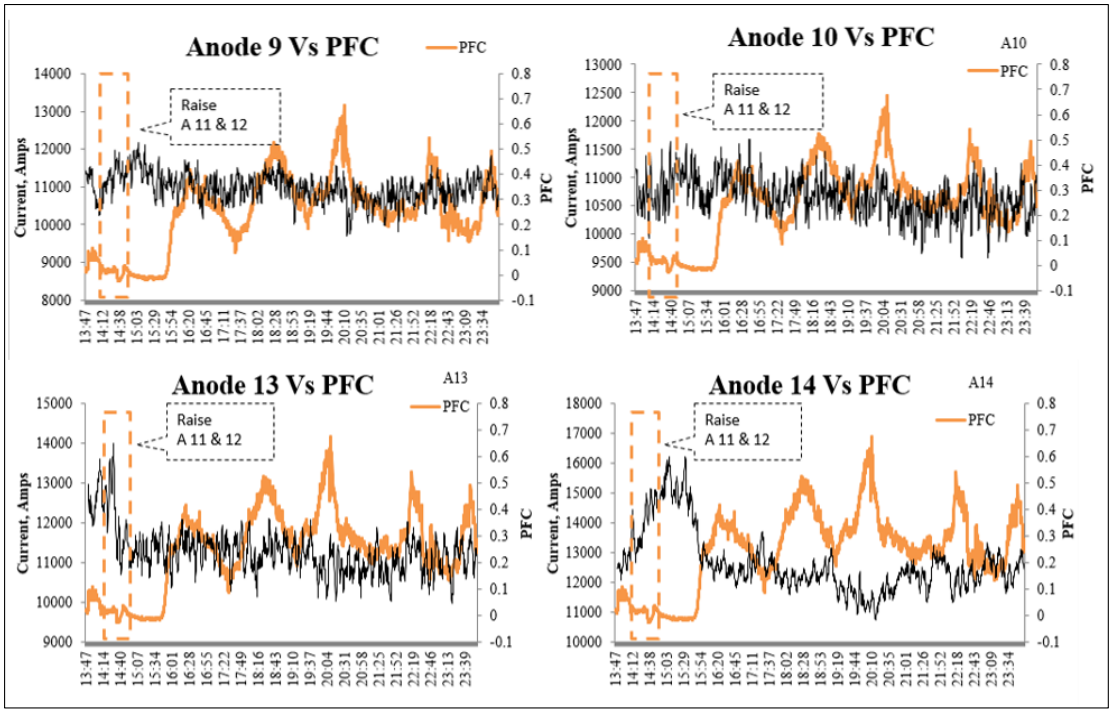

Figure 15. Anodes which shows current reduction and CF_4 increase while raising anodes 11 & 12 experiment.

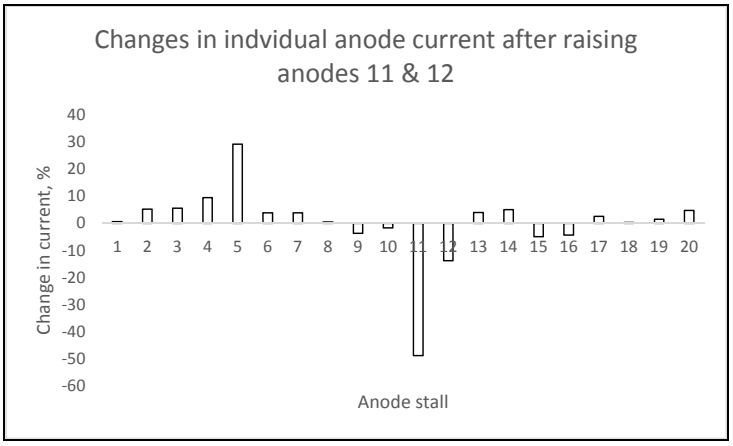

Figure 16. Current redistribution for two hours' time interval before and after raising anodes 11 & 12.

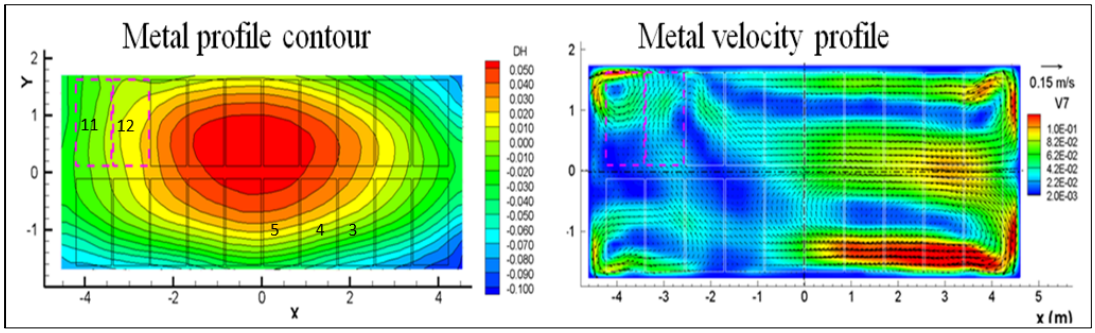

Figure 17. Changes in metal profile and velocity while replacing anodes 11 & 12 [9].

In the last part of the investigation, the impact of raising the pair of central anodes 4 and 5 by 1.0 cm was studied when both anode currents were reduced by 12 – 14 % due to the higher

inter-electrode distance as shown in Figure 18. Accordingly, the current was diverted toward other anodes which operate under lower ohmic resistance.

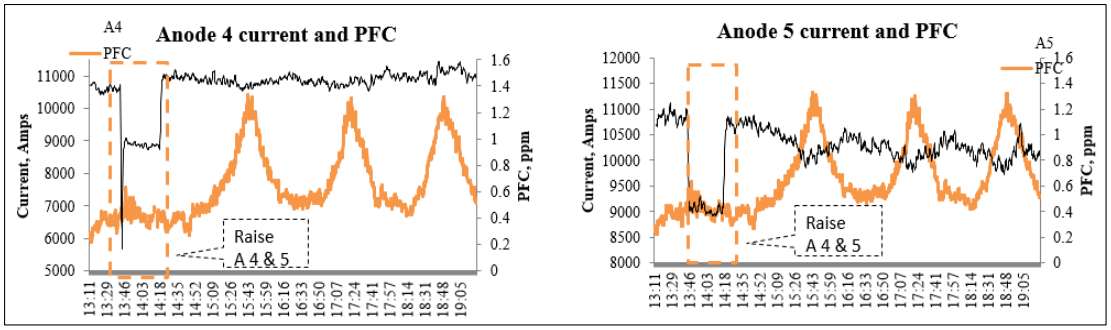

Figure 18. Changes in CF_4 emission and anodes 4 & 5 current while raising them.

The increase in current density of other anodes would raise their alumina depletion rate causing the formation of an alumina concentration gradient condition. Sequentially, this will result in the lowering of wettability of certain anodes and an increase in their current density as well as bubble coverage. Similar to the condition during the raising of corner anodes, polarising of certain anodes beyond the enabling limits of PFC formation will take place [21] as probably occurred for anode 6 in Figure 19 whilst its current experienced a partial reduction during the increase in PFC emission.

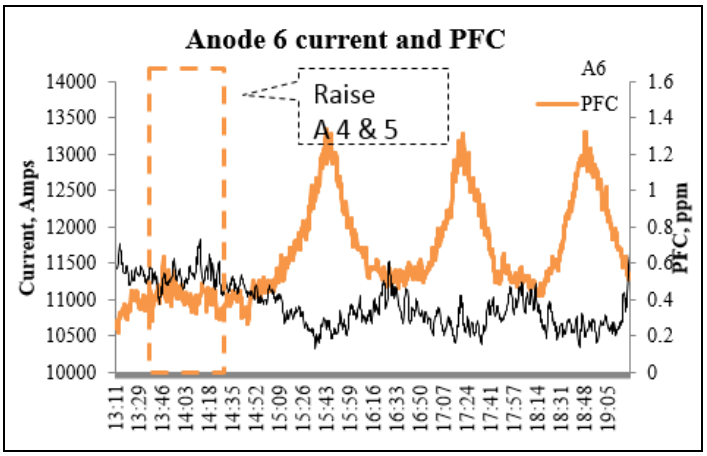

Figure 19. Neighbour anodes 6 current reduction along with CF_4 raise while raising anodes 4 & 5 experiment.

4. Conclusion

At lower energy input, the rate of current draw upon anode setting gets slower resulting in an extension of the period of operation under non-uniform current density while the current pick-up curve become individualistic based on stall location. The deterioration in cell thermal and electrical balance would be further prolonged during replacement of corner anodes due to slower anode current pick up rate compared to central anodes as a result of characteristic changes in local MHD and a higher heat loss at the corners of the cell. This work highlights these phenomena and provides opportunities to review work practise during anode setting with the possibility of setting different limits and energy input based on anode stall location.

The study has shown a quick response on the co-evolution of fluorocarbon species when introducing a spatial change in anode current density or alumina concentration in a modern cell and demonstrates the narrow operating window for an individual electrode operate prior to the onset of polarization. Co-evolution of fluorocarbon species appear very sensitive to imbalances in anode current distribution as they occurred soon after raising corner and central

anodes, illustrating the independent relation between generating PFC and location of anode stall imbalance. However, the impact of feeder blockage was different, with the study illustrating that the impact would be worse for a shortage in alumina supply from a corner feeders due to typical bath flow patterns which restrict alumina supply to corner anodes. The work should stimulate prospects for future development of controlling feeding algorithm in Hall-Héroult reduction cells based on feeder location and on-line monitored individual anode current signals.

5. References

1. A. Jassim, S. Akhmetov, B. J. Welch, M. Skyllas-Kazacos, J. Bao and Y. Yao, "Studies on Background PFC emission in Hall-Héroult reduction cells using online anode current signals," Presentation presented TMS Light Metals conference, FL, Orlando, 2015.
2. Z. Kuang, J. Thonstad and M. Sørlie, “Effects of Additives on the Electrolytic Consumption of Carbon Anodes in Aluminium Electrolysis”, Carbon, Vol.33, No.10, pp. 1479-1484, 1995.
3. M. Segatz, C. Droste and D. Vogelsang, "Magnetohydrodynamic effect of anode set pattern on cell performance," In Proceedings of TMS Light Metals, Orlando, FL, pp. 352–358, 1997.
4. J. Zoric, I. Rousar, and J. Thonstad, “Mathematical Modelling of industrial aluminium cells with prebaked anodes Part I: Current distribution and anode shape”, Journal of Applied Electrochemistry, vol. 27, pp. 916-927, 1997.
5. C.Y. Cheung et al. C. Menictas, J. Bao, M. Skyllas-Kazacos, and B. J. Welch, “Spatial Temperature Profiles in an Aluminium Reduction Cell under Different Anode Current Distributions,” In American Institute of Chemical Engineers (AIChE) 5(59), pp. 1544-1556, 2013.
6. R. V. Kaenel, J. Antille, M. V.Romerio, O. Besson, "Impact of magnetohydrodynamic and bubbles driving forces on the alumina concentration in the bath of an Hall-Héroult cell," In Proceeding of TMS Light Metals, San Antonio, pp. 585–590, 2013.
7. J.M. Purdie, Alumina Behaviour and Related Process Variation in Hall-Héroult Cells for Aluminium Production, PhD Thesis, University of Auckland, 1993.
8. A. Jassim, S. Akhmetov, B. J. Welch, M. Skyllas-Kazacos, J. Bao and Y. Yao, " Studies toward balancing the current in smelting cells," In Proceedings of 11th Australasian Aluminium Smelting Technology Conference, Dubai, 2014.
9. A. G. Arkhipov, "Calculation of metal heave and metal velocities for different AS patterns in D20 Technology," Internal presentation in Dubai Aluminium Dubai, 2011.
10. A. Solheim, "Practical implications of some interfacial processes in alumina reduction cells," In Proceedings of 11th Australasian Aluminium Smelting Technology Conference, Dubai, 2014.
11. A. Solheim, "Practical Implications of Some Interfacial Processes in Alumina Reduction Cells Energy Transfer and Product Formation at the Anode," Presentation presented 11th Australasian Aluminium Smelting Technology Conference, Dubai, 2014.
12. S. Fortin, M. Gerhardt, A.J. Gesing, "Physical modelling of bubble behaviour and gas release from aluminium reduction cells anodes," In Proceedings of TMS Light Metals, Los Angeles, CA, pp. 385–395, 1984.
13. L. I. Kiss and S. Poncsak, “Effect of the bubble growth mechanism on the spectrum of voltage fluctuations in the reduction cell,” In Proceedings of TMS Light Metals, Seattle, WA, pp. 217–223, 2002.
14. Y. Wang, L. Zhang, and X. Zuo, "Fluid Flow and Bubble Behavior in the Aluminum Electrolysis Cell," In Proceedings of TMS Light Metals, pp. 581–586, 2009.

15. D. Whitfild, S. Akhmetov, M. M. Al Jallaf, J. Balasques, K. Al Aswad, I. Baggash "From D18 to D18+: Progression of Dubal's original potlines," In Proceedings of TMS Light Metals, Orlando, FL, pp. 499–504, 2015.
16. M. M. R. Dorreen, Cell performance and anodic processes in aluminium smelting studied by product gas analysis. PhD thesis, The University of Auckland, 2000.
17. Chen X., Li W., Zhang Y, Q. "Investigation on formation mechanism of non-anode effect related PFC emissions from aluminium reduction cells," In Proceedings of TMS Light Metals, San Antonio, TX, pp. 877–881, 2013.
18. B. J. Welch, "Quantifying PFC emissions from smelter cells," In Proceedings of 10th Australasian Aluminium Smelting Technology Conference, Launceston, TAS, 2011.
19. L. Dion, C. L. Lagacé, J. W. Evans, R. Victor, and L. I. Kiss, "On-line Monitoring of Individual Anode Currents to Understand and Improve the Process Control at Alouette," In Proceedings of TMS Light Metals, Orlando, FL, pp . 723–728, 2015.
20. P. Meunier, Electrochemical Study of the Anode Effect in Aluminum Reduction Cells, PhD. thesis, University of New South Wales, 2006.
21. B.J. Welch, M. Iffert and M.Skyllas-Kazacos, "Reductions in the Carbon Dioxide Footprint of Aluminium Smelters by the Application of Fundamental Data", JOM, vol.60, No.11, November 2008, 17-24.
22. B. Moxnes, A. Solheim, M. Liane, E. Svinsås, and A. Halkjelsvik., "Improved cell operation by redistribution of the alumina feeding," In Proceedings of TMS Light Metals, pp . 461–466, 2009.
23. D. S. Wong, A. Tabereaux, P. Lavoie, "Anode effect phenomena during conventional AEs, low voltage propagating AEs & non-propagating AEs," In Proceedings of TMS Light Metals, San Antonio, TX, pp. 529–534, 2014.
24. Severo, D. S., Gusberti V. "A Modelling Approach to Estimate Bath and Metal Heat Transfer Coefficients", In Proceedings of TMS Light Metals, pp. 557-562, 2009.
25. Severo D. S., Gusberti V., Pinto E. C. V., Moura R. R., "Modeling the Bubble Driven Flow in the Electrolyte as a Tool for Slotted Anode Design Improvement", In Proceedings of TMS Light Metals, pp. 287-292, 2007.